Pak. J. Bot., 57(5): 1769-1777, 2025. DOI: http://dx.doi.org/10.30848/PJB2025-5(8)

GREEN SYNTHESIS AND SYNERGISTIC ANTIBACTERIAL ACTIVITY OF IRON OXIDE AND ALUMINUM OXIDE NANOPARTICLES USING *CYMBOPOGON CITRATUS* EXTRACT

INAM ULLAH KHAN[1], KASHIF BASHIR[2], ZARKISH TARIQ[3], WAJID SYED[4], FAIZ UR REHMAN[5*], MAHMOOD BASIL A. AL-RAWI[6], MOHEB ULLAH KHAN[7] AND KHUZIN DINISLAM[8]

[1]*Sarhad Institute of Allied Health Sciences (SIAHS), Sarhad University of Sciences and Information Technology Peshawar 25000 KPK Pakistan*
[2]*Department of Health and Biological Sciences Abasyn University Peshawar 25000 Peshawar Pakistan*
[3]*Department of Zoology, University of Science and Technology Bannu, Khyber Pakhtunkhwa, Pakistan*
[4]*Department of Clinical Pharmacy, College of Pharmacy, King Saud University, Riyadh 11451, Saudi Arabia*
[5]*Department of Zoology, Government Superior Science College Peshawar, 25000, Khyber Pakhtunkhwa, Pakistan*
[6]*Department of Optometry, College of Applied Medical Sciences, King Saud University, Riyadh, Saudi Arabia*
[7]*Department of biotechnology, University of science and technology bannu 28100 KP Pakistan*
[8]*Department of Chemistry, Bashkir State Medical University, Ufa, Russia*
[*]*Corresponding author's e-mail: faiz02140@gmail.com*

Abstract

Bioinspired synthesis of metal oxide nanoparticles (NPs) offers a sustainable alternative to conventional methods, promoting eco-friendly, cost-effective, and scalable production. Present study explores the synthesis and characterization of FeO and Al_2O_3 NPs using *Cymbopogon citratus* extract, followed by an evaluation of their synergistic antibacterial activity with conventional antibiotics against uropathogenic *Escherichia coli.* Utilizing the natural phytochemicals present in *C. citratus*, we successfully synthesized nanoparticles in a sustainable manner, eliminating the need for hazardous chemicals. The synthesized NPs were characterized using various techniques, revealing size and morphology variations. FeO-NPs exhibited a slightly spherical, porous morphology with a size range of 5-10 nm, while Al_2O3- NPs displayed a rod-like and granular structure with sizes ranging from 5-12 nm as per TEM analysis and broader distribution around 100 nm by Scanning Electron Microscopy (SEM). The study demonstrated enhanced antibacterial activity (10-100 fold) when these NPs were combined with various antibiotics (Amoxicillin-Clavulanic acid, Ampicillin, Co-trimoxazole, Ciprofloxacin, Amikacin, Imipenem, Chloramphenicol). The synergistic effect led to increased potency, with improvements ranging from 10-fold for Amoxicillin-Clavulanic acid to complete eradication (100% potency) of bacterial growth with Ampicillin. These findings highlight the potential of *C. citratus* extract for biogenic synthesis of FeO and Al_2O_3 NPs with promising antibacterial properties. Additionally, their synergistic effect suggests potential applications as antibiotic enhancers, paving the way for more effective treatments against uropathogenic *E. coli* infections

Key words*:* Biogenic synthesis, Synergistic antibacterial activity, Uropathogenic, *E. coli*, Antibiotic enhancers, Lemongrass extract, Metal oxide, Nanoparticles.

Introduction

Metal oxide nanoparticles (NPs) have garnered significant attention due to their unique physical and chemical properties, which make them valuable in fields such as medicine, biotechnology, environmental remediation, and antimicrobial applications (Chari *et al.*, 2017; Khan *et al.*, 2021; Sarkar *et al.*, 2022). Nanoparticles, typically ranging from 1 to 100 nm in size, exhibit distinctive structural features, including size, shape, and lattice structure, which enhance their functionality (Lei *et al.*, 2018).

Among metal oxide NPs, iron oxide nanoparticles (FeO-NPs) have been extensively studied for their applications in medicine (Gholami *et al.*, 2018), biotechnology (Katata-Seru *et al.*, 2018), environment (Jin *et al.*, 2018) and photocatalysis (Fatimah *et al.*, 2019). They are also effective antimicrobial agents against bacteria and fungi (Muthukumar *et al.*, 2019). However, conventional synthetic methods often rely on expensive and toxic chemicals, creating barriers for safe medical and environmental applications (Mohamed *et al.*, 2015). Green synthesis methods, particularly using plants, offer a sustainable alternative, utilizing phytochemicals as reducing and stabilizing agents to produce nanoparticles with minimal environmental impact (Makarov *et al.*, 2014; LewisOscar *et al.*, 2015; Sathiyavimal *et al.*, 2018).

Similarly, aluminum oxide nanoparticles (Al_2O_3-NPs) hold significant importance in antimicrobial applications, electrochemical sensors, and environmental remediation (Gbadamosi *et al.*, 2019; Manogar *et al.*, 2022; Wahab and Alam, 2022). Green synthesis of Al_2O_3-NPs has gained traction due to its eco-friendly approach, avoiding harsh chemicals and high-temperature processes while leveraging plant extracts or microorganisms (Bokhary *et al.*, 2022). Various studies have demonstrated the successful use of plant extracts for synthesizing Al_2O_3-NPs, such as those from *Muntingia calabura* (Sumesh and Kanthavel, 2019), Rosa (Goutam *et al.*, 2018), and *Citrus aurantium* peel (Nagarajan *et al.*, 2023), as well as grapefruit extract (Bokhary *et al.*, 2022).

Cymbopogon citratus (Lemon grass), a member of the Poaceae family, is widely recognized for its antibacterial, antioxidant, antifungal, and anticarcinogenic properties and is a promising candidate for green nanoparticle

synthesis (Bayala *et al.*, 2018; Ekpenyong *et al.*, 2015). Its phytochemicals, including geranial, neral, myrcene, and citral, play a crucial role in reducing, stabilizing, and functionalizing metal oxide precursors (Almeida *et al.*, 2019; Bayala *et al.*, 2018). Additionally, lemongrass essential oil has demonstrated antibacterial activity against multidrug-resistant bacteria, including methicillin-resistant *Staphylococcus aureus* (Manvitha & Bidya, 2014; Sharma *et al.*, 2013).

The emergence of multidrug-resistant bacteria presents a severe global health challenge (Rossolini *et al.*, 2014), rendering many antibiotics ineffective and necessitating alternative therapeutic strategies (Lin *et al.*, 2015; Ventola, 2015). Recent studies on biologically synthesized nanoparticles, such as FeO-NPs and Al_2O_3 NPs, offer a viable solution due to their potent antimicrobial activity and biocompatibility (Muzammil *et al.*, 2020). Biocompatible FeO-NPs synthesized using plant extracts, such as *Ageratum conyzoides* and *Cynometra ramiflora*, have shown promising results in photocatalysis, antibacterial activity, and environmental remediation (Groiss *et al.*, 2017; Madivoli *et al.*, 2019). Similarly, Al_2O_3-NPs exhibited significant antibacterial properties, alongside applications in biosensors, (Liu *et al.*, 2011), biofiltration, and drug delivery (Monteiro-Riviere *et al.*, 2010). Their effectiveness against various bacterial strains further underscores their biological potential (Ansari *et al.*, 2015; Balasubramanyam *et al.*, 2010; Mukherjee *et al.*, 2011). These findings emphasize the importance of biologically synthesized metal oxide nanoparticles in combating multidrug-resistant bacteria and addressing environmental challenges.

Green synthesis of FeO and Al_2O_3-NPs using *C. citratus* extract results in eco-friendly nanoparticles with enhanced antibacterial properties, providing a sustainable approach to combat multidrug-resistant bacteria and environmental contaminants.

Therefore, the present study aims to explore the green synthesis, characterization, and bio-evaluation of FeO and Al_2O_3-NPs using *C. citratus* extract. By leveraging the phytochemicals in *C. citratus*, this research seeks to develop eco-friendly nanoparticles with enhanced antibacterial activity, offering a sustainable approach to addressing the challenges posed by multidrug-resistant bacteria and environmental contaminants.

Material and Method

Study design: The present study was carried out at the Microbiology Research Laboratory (MRL), Abasyn University, and Peshawar, Pakistan

Collection and identification: *Cymbopogon citratus* plants were collected during the December 2022 from the National Institute of Food and Agriculture (NIFA), Peshawar, Pakistan. The plants were identified to ensure accurate species identification (Ali & Qaiser,1993-2018; Khan & Badshah, 2019).

Drying of plant: Following collection, *C. citratus* leaves were thoroughly washed with tap water to remove any adhering dust or dirt. The leaves were then chopped into small pieces and shade-dried at room temperature. This method helps to maintain the quality and essential oil content of the leaves, which are sensitive to heat and high temperatures (Coradi *et al.*, 2014). After drying, the leaves were ground into a fine powder using a grinder and stored in airtight polyethylene bags for further use.

Collection of *E. coli*: A confirmed uropathogenic strain of Escherichia coli was obtained from the Institute of Kidney Disease (IKD) Peshawar, Pakistan.

Preparation of aqueous extract of *Cymbopogon citratus* leaves: For the preparation of the aqueous extract, 25 g of the powdered *C. citratus* leaves were weighed and mixed with 100 mL of sterile, distilled water in a 250 mL beaker. The mixture was then heated to 100°C for 10 minutes with continuous stirring to facilitate the extraction of bioactive compounds. After cooling, the reaction mixture was centrifuged at 12000 rpm for 10 minutes to remove any solid debris. The supernatant was then filtered sequentially using a 0.45 µm polytetrafluoroethylene (PTFE) membrane filter followed by a sterile 0.2 µm Millipore membrane filter. The final filtrate, containing the *C. citratus* extract, was stored at 4°C for further use as a stabilizing and capping agent during nanoparticle synthesis (Ansari *et al.*, 2015; Patiño-Ruiz *et al.*, 2020).

Synthesis of iron oxide NPs: For the synthesis of FeO-NPs, 40 mL of 0.26 M ferric chloride hexahydrate ($FeCl_3$-$6H_2O$) solution was combined with 40 mL of the prepared *C. citratus* extract under constant stirring at room temperature. To minimize oxygen intrusion, the solution was then heated to 60°C for 1 hour. Subsequently, an additional 40 mL of 0.52 M $FeCl_3$-$6H_2O$ solution, prepared in distilled water, was added drop wise to the reaction mixture while maintaining continuous stirring. The temperature was then gradually raised to 85°C. To achieve a final pH of 10, promoting nanoparticle precipitation, 15 mL of 0.75 M sodium carbonate (Na_2CO_3) solution was added drop wise. The reaction mixture turned dark brown after the addition of Na_2CO_3, indicating the formation of FeO-NPs. The dark brown precipitates were collected by centrifugation and washed repeatedly with distilled water to remove any residual impurities. The FeO-NPs were further washed with ethanol for additional purification. Finally, the purified FeO-NPs were dried in an oven at 70°C for 24 hours (Patiño-Ruiz *et al.*, 2020).

Synthesis of aluminum oxide NPs: Aluminum nitrate nonahydrate ($Al(NO_3)3•9H_2O$) was used as a precursor for the synthesis of Al_2O_3-NPs via the boehmite route. Briefly, 20 mL of the *C. citratus* extract was added to 80 mL of a boehmite solution under stirring at 37°C. The mixture was then subjected to microwave irradiation as described by (Ansari *et al.*, 2015), microwave irradiation of the combination solution was permitted. The resulting Al_2O_3-NPs were isolated and purified by centrifugation.

Characterization of the Nano particles: The morphology and size of the synthesized nanoparticles were examined using Scanning Electron Microscopy (SEM). The internal structure and size distribution were further investigated using Transmission Electron Microscopy (TEM). Energy-dispersive X-ray spectroscopy (EDX), coupled with SEM, was employed to determine the elemental composition of

the nanoparticles. X-ray diffraction (XRD) analysis was performed to identify the crystalline phases present in the nanoparticles. Finally, UV-Vis spectroscopy was used to characterize the optical properties of the nanoparticles. Specific parameters used for each technique will be provided upon instrument availability. The nanoparticles will also be stored under controlled conditions (e.g., desiccated environment) to minimize any potential degradation (Ansari *et al.*, 2015).

Antibiotic susceptibility profile of *E. coli*: Antibiotic susceptibility testing against *E. coli* was performed using the disc diffusion assay. Bacterial turbidity was adjusted to McFarland 0.5 standard. Sterile cotton swabs were used to create a uniform lawn on nutrient agar plates, and antibiotic discs were placed on the prepared lawn with sterilized forceps. The inoculated plates were incubated at 37°C for 24 hours. Zones of inhibition were measured in millimeters according to standard guideline (Weinstein & Lewis, 2020). The list of antibiotics used is provided in Table 1.

Table 1. List of Antibiotics used.

S. No.	Antibiotics	Concentration (µg)
1	Amoxacillin-clavulanic acid	30µg
2.	Ampicillin	10µg
3.	co-trimoxazole	10µg
4.	Chloramphenicol	30µg
5.	Ciprofloxacin	5µg
6.	Impenem	10µg
7.	Amikacin	30µg

Antibacterial activity of NPs against *E. coli:* The antibacterial activity of the synthesized nanoparticles was evaluated using the agar well diffusion method. Bacterial suspensions were prepared in normal saline, and a loopful of each isolate was inoculated on Muller Hinton agar plates. Wells (6mm) were bored using a sterile cork borer. One well was used for the negative control (distilled water), one for the positive control (Ciprofloxacin), and the third for the test material (nanoparticles). The plates were sealed with parafilm and incubated at 37°C for 24 hours. Zones of inhibition were measured in millimeters (Saeb *et al.*, 2014).

Synergistic effect of nanoparticles: The synergistic effect of the nanoparticles with antibiotics was determined by placing equal amounts of nanoparticles and antibiotics on plates containing *E. coli*. The plates were incubated at 37°C for 24 hours, and the zones of inhibition were measured.

Nanoparticles, extract and its synergistic activity (MIC, FIC and FICI): The minimum inhibitory concentration (MIC) of the nanoparticles was determined using the agar well diffusion method with different concentrations (10µl, 20µl, and 30µl) of nanoparticles alone and in combination with antibiotics. Nutrient agar medium was prepared and poured into sterile petri dish followed by inoculation of fresh bacteria. Sterile cork borers will be used to create wells (6 mm diameter) in the agar. The inoculated plates will be incubated at 37°C for 24 hours. Following incubation, the diameters of the clear zones of inhibition surrounding each well will be measured in millimeters (Parvekar *et al.*, 2020).

For the evaluation of synergistic activity, Fractional inhibitory concentration (FIC) and Fractional inhibitory concentration Index (FICI) were determined using the following formulae (Buyck *et al.*, 2015).

$FIC_{ab} = MIC_{(ab\ combination)} / MIC_{(ab\ alone)}$
$FIC_{extract} = MIC_{(extract\ in\ combination)} / MIC_{(extract\ alone)}$

While FIC index was the sum of FIC of both NPs.

$$FICI = FIC_{ab} + FIC_{extract}$$

In case of two or more extracts combination FIC was calculated as per following formula (Hall *et al.*, 1983).

$$FICI = (A/Ma) + (B/Mb)$$

Ma and Mb are individual MICs of test compounds in synergistic.

The values obtained from the application of above formulae were used to grade the combinations to be additive (>0.5 to 1), synergistic (≤0.5), NPs (≥2) or in different (>1 to <2) in their potential.

Statistical analysis of the data: Microsoft Excel was used for statistical analysis (Dianat *et al.*, 2015).

Results

Green synthesis of iron oxide and aluminum oxide NPs: Iron oxide nanoparticles (FeO-NPs) and aluminum oxide nanoparticles (Al_2O_3-NPs) were successfully synthesized using an aqueous extract of *C. citratus* leaves. Different analytical techniques such as EDX spectroscopy along with SEM and TEM were used. The crystal structure was determined by using XRD while the concentration of compounds in the mixture was measured by UV-Vis spectroscopy for the characterization of FeO-NPs and Al_2O_3-NPs.

TEM of FeO-NPs and Al_2O_3-NPs: TEM images (Fig. 1) revealed that FeO-NPs were slightly spherical and highly porous with a surface area of 22.5 m2/g, which is four times higher than commercially available hematite NPs.

The Al_2O_3-NPs exhibited a rod- and grain-shaped morphology with a size of up to 12 nm. These nanoparticles displayed a tendency to form clusters (Fig. 2). As a result, the Al_2O_3-NPs in the solution ought to be equally distributed.

UV-Vis spectrophotometry: The UV-Vis spectra (Fig. 3) confirmed the presence of FeO-NPs in the solution. The observed peak at 460 nm can be attributed to the electronic transitions within the FeO-NPs. Specifically, the absorption peak around 460 nm is associated with ligand-to-metal charge transfer (LMCT) transitions from the oxygen ligands to the iron centers, which is consistent with previous studies (Hussain *et al.*, 2023; Thahab *et al.*, 2020). Analysis of the UV-Vis spectrum of the synthesized FeO-NPs revealed that they were formed in a solution with a 1:2 ratio, where 10 mL of plant extract was mixed with 5 mL of FeO-NPs solution.

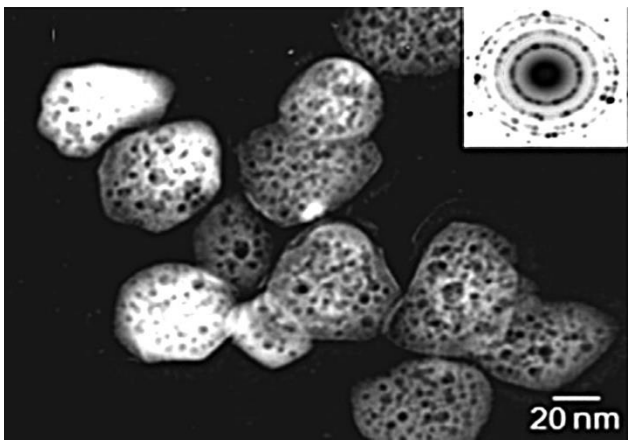

Fig. 1. TEM image of FeO-NPs synthesized.

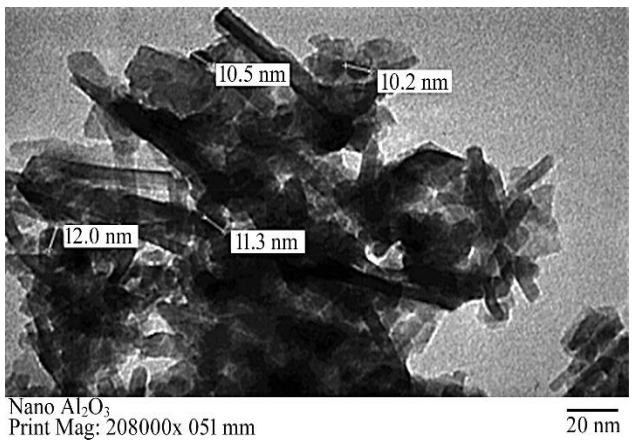

Fig. 2. TEM images of Al_2O_3-NPs.

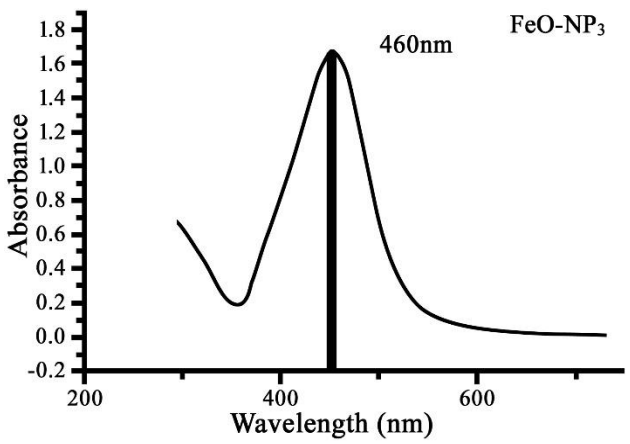

Fig. 3. UV-vis Spectrum of synthesized FeO.

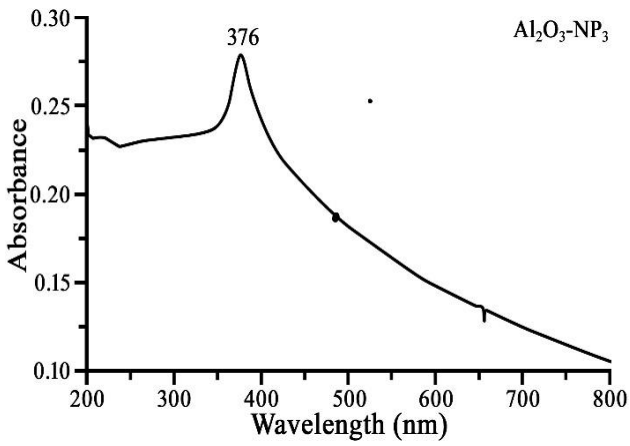

Fig. 4. UV-Vis Spectrum of Synthesized Al_2O_3-NPs.

Fig. 5. SEM Image of FeO-NPs of *C. citratus* Leaves extract.

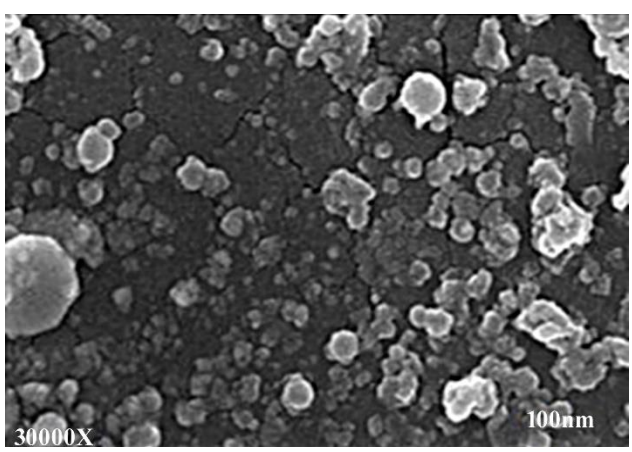

Fig. 6. SEM image of Al_2O_3-NPs of *C.citratus* leaves.

A characteristic peak at 450 nm was observed, indicating the presence of Al_2O_3-NPs. UV-Vis spectroscopy revealed that the sample absorbed energy and exhibited a characteristic peak at 450 nm. Additionally, a peak at 376 nm suggested the high purity of the nanoparticles (Fig. 4).

Scanning electron microscopy (SEM): SEM images (Fig. 5) corroborated the TEM findings, showing FeO-NPs with a spherical morphology and a size range of 5-10 nm.

Images showed Al_2O_3-NPs in the range of 100 nm at a magnification of 30,000X (Fig. 6). While larger than FeO-NPs, the results suggest the *C. citratus* extract influenced the formation of irregular shaped Al_2O_3-NPs.

Energy Dispersive X-ray Analysis (EDX): EDX analysis (Fig. 7) confirmed the presence of iron (Fe) and oxygen (O) in the synthesized FeO-NPs, indicating successful synthesis. The graph also displayed the presence of Oxygen while carbon and Sulphur in lesser amount.

EDX analysis of the Al_2O_3-NPs revealed aluminum (Al) and oxide were present in the sample as shown in (Fig. 8). The graph also displayed the presence of Oxygen while silver in lesser amount.

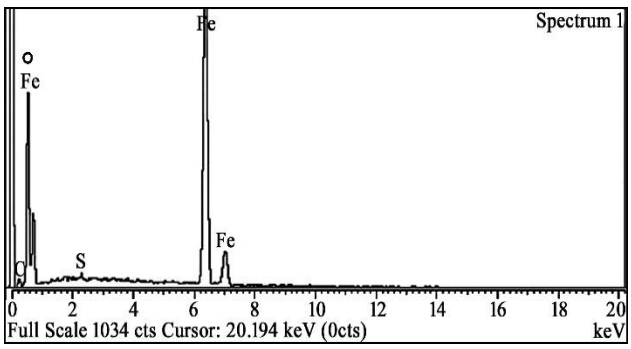

Fig. 7. EDX Spectrums of synthesized FeO-NPs.

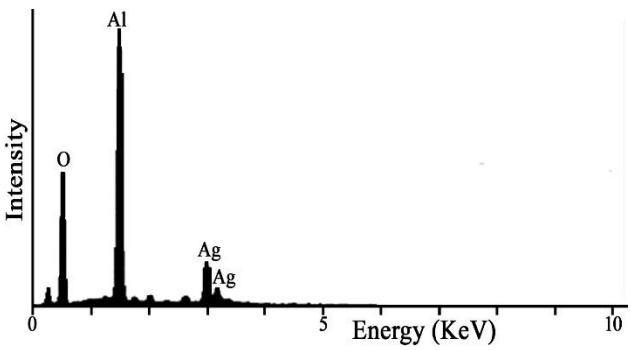

Fig. 8. Energy Dispersive X-Ray Analysis (EDX) of Al_2O_3-NPs

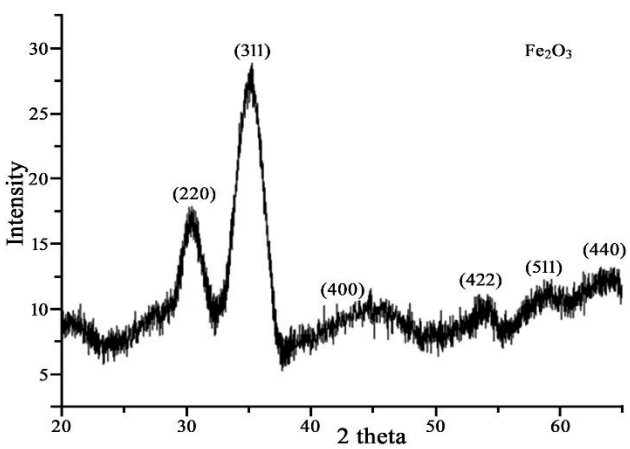

Fig. 9. XRD Spectrums of the synthesized FeO-NPs.

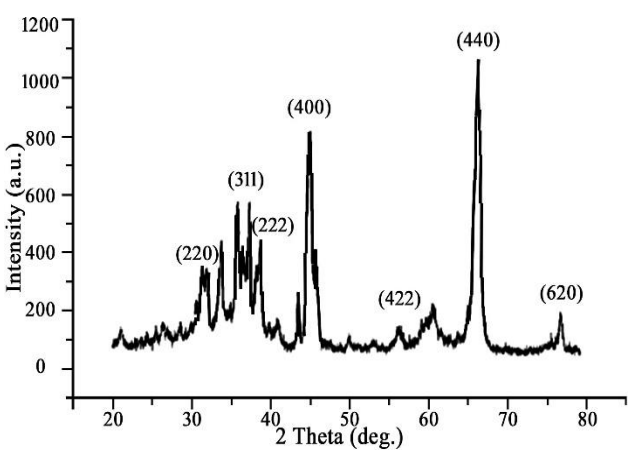

Fig. 10. XRD Spectra Displaying Crystalline like of Al_2O_3

X-ray Diffraction (XRD) Analysis FeO-NPs: The phase purity and composition of the products obtained by the biosynthesis using leaves extract of *C. citratus* by XRD. XRD patterns (Fig. 9) revealed the crystalline nature of the FeO-NPs. The diffraction peaks were indexed to the (311) reflection planes of the FeO crystal structure.

XRD spectrum of synthesized Al_2O_3 NPs (Fig. 10). Analysis of XRD spectrum exposed that the sample was finely ground and homogenized material. This indicates the crystalline nature of the Al_2O_3-NPs. The four distinct diffraction peaks at 2θ values of 44° and 62° can be indexed to the (620) reflection planes of a cubic structure. However, the presence of additional peaks at 422°, 400°, 311°, and 222° suggests the presence of organic contaminants.

FeO-NPs Activity of Coated and Non-Coated Antibiotic against *E. coli:* The antibacterial activity of FeO-NPs and Al_2O_3-NPs, synthesized using *C.citratus* extract (as described in the methodology), was evaluated against *E. coli* by measuring the zone of inhibition of coated and uncoated antibiotic discs. Coating antibiotic discs with FeO-NPs generally enhanced their antibacterial activity against *E. coli.*

Uncoated Amoxicillin Clavulanic Acid and Ampicillin discs showed no inhibition (0 mm), but FeO-NPs coating increased the zones to 10 mm, representing a 100% potency increase.

Co-trimoxazole and Ciprofloxacin exhibited notable enhancements, with their zones increasing from 14 mm to 24 mm (71.4%) and 15 mm to 29 mm (93.3%), respectively.

Moderate increases were observed for Amikacin (15 mm to 20 mm, 33.3%) and Chloramphenicol (15 mm to 20 mm, 33.3%). The most significant improvement was seen with Imipenem, where the zone rose from 27 mm to 37 mm, representing a 37% increase in potency (Table 2).

Al_2O_3-NPs activity of coated and non-coated antibiotics against *E. coli*: Similarly, Al_2O_3-NPs coating improved the antibacterial performance of all antibiotics. Amoxicillin Clavulanic Acid and Ampicillin showed zones of inhibition of 8 mm and 9 mm, respectively, compared to 0 mm for uncoated discs, reflecting a 100% increase.

Co-trimoxazole exhibited a moderate increase from 14 mm to 20 mm (42.8%). Modest improvements were noted for Ciprofloxacin (15 mm to 17 mm, 13.3%), Amikacin (15 mm to 18 mm, 20%), and Chloramphenicol (15 mm to 17 mm, 13.3%).

Imipenem displayed the highest increase among the tested antibiotics, with the zone expanding from 27 mm to 34 mm (25.9%) (Table 3).

Antibacterial activity of the synthesized NPs: The antibacterial activity of the synthesized FeO-NPs and Al_2O_3-NPs was evaluated against *E. coli* using the disc diffusion assay (Table 4). Both FeO-NPs and Al_2O_3-NPs extracts demonstrated good antibacterial activity. FeO-NPs extract exhibited a maximum zone of inhibition of 17 mm at a concentration of 100 µl, while Al_2O_3-NPs extract showed a maximum zone of inhibition of 19 mm at the same concentration. DMSO served as the negative control, while ciprofloxacin was used as the positive control (Table 3).

Table 2. FeO-NPs activity of coated and non-coated antibiotics against *E. coli*.

Antibiotic used in activity		Zone of inhibition (mm)	Increased potency%
Amoxicillin Clavulanic acid	Uncoated	0	100%
	FeO-NPs coated	10	
Ampicillin	Uncoated	0	100%
	FeO-NPs coated	10	
Co-trimoxazole	Uncoated	14	71.4%
	FeO-NPs coated	24	
Ciprofloxacin	Uncoated	15	93.3%
	FeO-NPs coated	29	
Amikacin	Uncoated	15	33.3%
	FeO-NPs coated	20	
Impenem	Uncoated	27	37%
	FeO-NPs coated	37	
Chloramphenicol	Uncoated	15	33.3%
	FeO-NPs coated	20	

Table 3. Al_2O_3-NPs activity of coated and non-coated antibiotics against *E. coli*.

Antibiotic used in activity		Zone of inhibition (mm)	Increased potency%
Amoxicillin Clavulanic acid	Uncoated	0	100%
	Al_2O_3-NPs coated	08	
Ampicillin	Uncoated	0	100%
	Al_2O_3-NPs coated	09	
Co-trimoxazole	Uncoated	14	42.8%
	Al_2O_3-NPs coated	20	
Ciprofloxacin	Uncoated	15	13.3%
	Al_2O_3-NPs coated	17	
Amikacin	Uncoated	15	20%
	Al_2O_3-NPs coated	18	
Imipenem	Uncoated	27	25.9%
	Al_2O_3-NPs coated	34	
Chloramphenicol	Uncoated	15	13.3%
	Al_2O_3-NPs coated	17	

Table 4. Antibacterial activity of Al_2O_3-NPs and FeO-NPs against *E. coli*.

Fractions	Conc.	Zone of inhibition in millimeter (mm)		
		E. coli	-ve DMSO control	+ve Control ciprofloxacin
Al_2O_3-NPs	100µl	19 ± 0.56	0	15
FeO-NPs	100µl	17 ± 0.56	0	16

Discussion

Green technology for the production of Al_2O_3 and FeO nanoparticles (Al_2O_3-NPs and FeO-NPs) has gained significant importance in recent years due to its simple, non-toxic, time-efficient, and cost-effective nature (Nagarajan *et al.*, 2013). Our findings on the antibacterial properties of these green-synthesized nanoparticles contribute to the existing body of research, as highlighted by (Madivoli *et al.*, 2019), demonstrating the potential application of Al_2O_3-NPs and FeO-NPs in pharmaceutical and cosmetic products. The characterization of these nanoparticles was conducted using various techniques, including UV-Vis spectroscopy, scanning electron microscopy (SEM), energy-dispersive X-ray spectroscopy (EDX), and X-ray diffraction (XRD). Further studies to quantify the antibacterial activity against specific pathogens are warranted to confirm this potential.

In present study, the UV-Vis absorption spectrum of FeO-NPs and Al_2O_3-NPs exhibited characteristic peaks at 460 nm and 376 nm, respectively, confirming the successful synthesis of these nanoparticles, as supported by previous findings (Groiss *et al.*, 2017) EDX analysis further verified the presence of iron and oxygen in FeO-NPs, corroborating their synthesis. SEM imaging revealed distinct spherical particles, while XRD analysis confirmed the crystalline structure of FeO-NPs, with the absence of additional peaks indicating high purity. Variations in absorption peak positions within the 300–500 nm range have been reported in other studies (Hussain *et al.*, 2023; Thahab *et al.*, 2020). Hussain *et al.* (2023) observed peaks for iron oxide nanoparticles in the range of 230–290 nm, significantly different from the 460 nm peak observed in this study. These discrepancies are likely due to differences in synthesis protocols, including variations in precursor concentration, temperature, and pH, which influence particle size, surface properties, and, consequently, the absorption spectra. Similarly, Thahab *et al.* (2020) reported absorption peaks at 292 nm for Fe-NPs and 363 nm for FeO-NPs, demonstrating that nanoparticle type significantly impacts the absorption spectrum. These findings, alongside our results, emphasize the role of synthesis conditions in shaping the optical characteristics of nanoparticles. Saleh *et al.* (2023) further demonstrated the applicability of UV-Vis spectroscopy for detecting Al_2O_3-NPs, highlighting its utility in nanoparticle characterization. Although their work did not specify peak values, it reinforces the technique's relevance for Al_2O_3-NP identification. The variations in absorption peaks reported across different studies underscore the complexity of nanoparticle synthesis and the pressing need for standardized protocols to achieve consistent and reproducible optical properties.

Characterization through SEM revealed mono-dispersed FeO-NPs with an irregular morphology and an average size of 50 nm, suggesting the involvement of biomolecules in the *C. citratus* extract as reducing agents. This finding aligned with Ansari *et al.* (2015), who reported spherical Al_2O_3-NPs synthesized using *C. citratus* extract with an average size of 34.5 nm. The observed variations in nanoparticle morphology and size between studies highlight the influence of synthesis parameters and metal oxide types on nanoparticle properties. These structural differences could also impact the antibacterial efficacy of the nanoparticles, a hypothesis supported by Azam *et al.*, (2012), who demonstrated that smaller nanoparticles with higher surface-to-volume ratios exhibited enhanced antimicrobial activity. Future studies optimizing synthesis conditions are crucial for tailoring nanoparticle properties for specific applications.

In this study, the observed antibacterial activity of the Al_2O_3 and FeO nanoparticles cannot be definitively attributed to the green synthesis approach due to the lack of direct evidence. However, biomolecules in *C. citratus* extract are likely to influence nanoparticle size and surface

characteristics, enhancing antibacterial effects. This aligns with reports by Rufus *et al*., (2017) and Olawade *et al*., (2024), which emphasize the importance of biomolecule-mediated synthesis in enhancing nanoparticle properties. Specifically, Olawade *et al*., (2024) detailed that the generation of reactive oxygen species (ROS) and membrane disruption are key antimicrobial mechanisms of nanoparticles. These findings support our hypothesis that the green synthesis approach contributed to the enhanced antibacterial effects observed in this study.

In our study, the Al_2O_3 NPs exhibited a larger zone of inhibition (19 mm) compared to the iron oxide nanoparticles (FeO-NPs) (17 mm) at the same concentration (100 µl), suggesting a higher efficacy against *E. coli*. This finding aligned with Ansari *et al*., (2015), who reported the effectiveness of green-synthesized Al_2O_3-NPs using *C. citratus* extract against *P. aeruginosa*. Similarly, the observed activity of FeO-NPs is consistent with Groiss *et al*., (2017) who demonstrated their efficacy against *E. coli* and *S. epidermidis* and Hussain *et al*., (2023), who reported substantial antimicrobial potential of iron oxide nanoparticles against various bacterial strains. Focusing on FeO-NPs, our research confirmed their ability to enhance the efficacy of various antibiotics against *E. coli*. Uncoated antibiotics displayed minimal to no inhibition zones, whereas FeO-NPs coating significantly increased their potency. This increase ranged from 33.3% for Amikacin and Chloramphenicol to 93.3% for Ciprofloxacin. This enhancement highlights the potential synergistic effects of nanoparticles and antibiotics, necessitating further investigation into these interactions. However, Madivoli *et al*., (2019) observed only moderate antibacterial activity of FeO-NPs synthesized using a different plant extract, highlighting that the choice of plant extract and synthesis conditions significantly influenced the characteristics and antibacterial efficacy of FeO-NPs. This finding emphasizes the need to optimize synthesis parameters and select suitable plant extracts to produce consistent and effective antibacterial nanomaterials. Furthermore, our work complements Manikandan *et al*., (2019) by focusing on the impact of Al_2O_3-NPs on *E. coli*, a prevalent gram-negative bacterium. While their research explored the broad-spectrum activity of biogenic Al_2O_3-NPs, we quantified the improvement in efficacy for various antibiotics. Interestingly, similar to β-lactams, we observed a substantial increase in the zone of inhibition for Imipenem and Co-trimoxazole, while Ciprofloxacin and Amikacin showed a more moderate enhancement. This suggests that the interaction between Al_2O_3-NPs and different antibiotics may influence the degree of efficacy improvement, need further investigation.

These results, along with findings by Muzammil *et al*., (2020), support the potential of FeO and Al_2O_3 NPs as antibacterial agents. While our study suggests that green synthesis contributes to these effects, direct evidence linking biomolecules in the extract to enhanced antibacterial activity is limited. Further investigations are necessary to elucidate the exact mechanisms by which the green synthesis method impacts these characteristics. Advanced analytical techniques, could provide additional insights into the role of biomolecules in nanoparticle synthesis and their interaction with bacterial membranes.

Conclusion

The green synthesis of Al_2O_3-NPs and FeO-NPs using *C. citratus* extract demonstrated significant antibacterial activity against *E. coli*. While the findings underscore the potential of plant-based nanoparticle synthesis for biomedical applications, further studies are required to optimize synthesis parameters, standardize characterization methods, and investigate the specific antimicrobial mechanisms at play. These efforts will contribute to the development of more effective and environmentally sustainable antibacterial agents.

Acknowledgment

The authors of this study extend their appreciation to Researchers Supporting Project (Project number RSP2025R378), King Saud University, Riyadh, Saudi Arabia.

References

Ali, S.I. and M. Qaiser (Eds.). 1993-2018. Flora of Pakistan, Department of Botany, University of Karachi, Karachi.

Almeida, K.B., A.S. Ramos, J.B.B. Nunes, B.O. Silva, E.R.A. Ferraz, A.S. Fernandes, I. Felzenszwalb, A.C.F. Amaral, V.G. Roullin, and D.Q. Falcão. 2019. PLGA nanoparticles optimized by Box-Behnken for efficient encapsulation of therapeutic *Cymbopogon citratus* essential oil. *Coll. Surf. Biointerf.*, 181: 935-942.

Ansari, M.A., H.M. Khan, M.A. Alzohairy, M. Jalal, S.G. Ali, R. Pal and J. Musarrat. 2015. Green synthesis of Al2O3 nanoparticles and their bactericidal potential against clinical isolates of multi-drug resistant Pseudomonas aeruginosa. *World J. Microbiol. Biotechnol*., 31(1): 153-164.

Azam, A., A.S. Ahmed, M. Oves, M.S. Khan, S.S. Habib and A. Memic. 2012. Antimicrobial activity of metal oxide nanoparticles against Gram-positive and Gram-negative bacteria: A comparative study. *Int. J. Nanomed*., 7: 6003-6009.

Balasubramanyam, A., N. Sailaja, M. Mahboob, M.F. Rahman, S.M. Hussain and P. Grover. 2010. *In vitro* mutagenicity assessment of aluminium oxide nanomaterials using the Salmonella/microsome assay. *Toxicol. In Vitro*, 24(6): 1871-1876.

Bayala, B., I.H.N. Bassole, S. Maqdasy, S. Baron, J. Simpore and J.-M.A. Lobaccaro. 2018. *Cymbopogon citratus* and Cymbopogon giganteus essential oils have cytotoxic effects on tumor cell cultures. *Biochimie*, 153: 162-170.

Bokhary, K.A., F. Maqsood, M. Amina, A. Aldarwesh, H.K. Mofty and H. M. Al-yousef. 2022. Grapefruit extract-mediated fabrication of photosensitive aluminum oxide nanoparticles and their antioxidant and anti-inflammatory potential. *Nanomaterials*, 12(11): 1885.

Buyck, J.M., P.M. Tulkens and F. Van Bambeke. 2015. Activities of antibiotic combinations against resistant strains of *Pseudomonas aeruginosa* in a model of infected THP-1 monocytes. Antimicrob. *Agents Chemother*., 59(1): 258-268.

Chari, N., L. Felix, M. Davoodbasha, A.S. Ali and T. Nooruddin. 2017. *In vitro* and in vivo antibiofilm effect of copper nanoparticles against aquaculture pathogens. *Biocatal. Agric. Biotechnol*., 10: 336-341.

Coradi, P.C., E. de Castro Melo and R.P. da Rocha. 2014. Mathematical modeling of the drying kinetics of the leaves of lemon grass (*Cymbopogon citratus* Stapf) and its effects on quality. *Idesia*, 32(4): 43-56.

Dianat, O., S. Saedi, M. Kazem and M. Alam. 2015. Antimicrobial activity of nanoparticle calcium hydroxide against *Enterococcus faecalis*: An *In vitro* study. *Iran. Endod. J*., 10(1): 39.

Ekpenyong, C.E., E. Akpan and A. Nyoh. 2015. Ethnopharmacology, phytochemistry, and biological activities of *Cymbopogon citratus* (DC.) Stapf extracts. *Chin. J. Nat. Med*., 13(5): 321-337.

Fatimah, I., S.N. Amaliah, M.F. Andrian, T.P. Handayani, R. Nurillahi, N. I. Prakoso, W. P. Wicaksono, and L. Chuenchom. 2019. Iron oxide nanoparticles supported on biogenic silica derived from bamboo leaf ash for rhodamine B photodegradation. *Sustain. Chem. Pharm*., 13: 100149.

Gbadamosi, A.O., R. Junin, M.A. Manan, A. Agi, J.O. Oseh and J. Usman. 2019. Synergistic application of aluminium oxide nanoparticles and oilfield polyacrylamide for enhanced oil recovery. *J. Pet. Sci. Eng*., 182: 106345.

Gholami, L., R. Kazemi Oskuee, M. Tafaghodi, A. Ramezani Farkhani, and M. Darroudi. 2018. Green facile synthesis of low-toxic superparamagnetic iron oxide nanoparticles (SPIONs) and their cytotoxicity effects toward Neuro2A and HUVEC cell lines. *Ceram. Int*., 44(8): 9263-9268.

Goutam, S.P., A.S. K., M. Yadav, D. Roy and R. Shastri. 2018. Green synthesis and characterization of aluminium oxide nanoparticles using leaf extract of Rosa. *Adv. Sci. Eng. Med*., 10(7): 719–722.

Groiss, S., R. Selvaraj, T. Varadavenkatesan and R. Vinayagam. 2017. Structural characterization, antibacterial and catalytic effect of iron oxide nanoparticles synthesised using the leaf extract of Cynometra ramiflora. *J. Mol. Struct*., 1128: 572-578.

Hall, M.J., R.F. Middleton and D. Westmacott. 1983. The fractional inhibitory concentration (FIC) index as a measure of synergy. *J. Antimicrob. Chemother*., 11(5): 427–433.

Hussain, A., M. Yasar, G. Ahmad, M. Ijaz, A. Aziz, M.G. Nawaz, F.A. Khan, H. Iqbal, W. Shakeel, H. Momand and others. 2023. Synthesis, characterization, and applications of iron oxide nanoparticles. *Int. J. Health Sci*., 17(4): 3.

Jin, X., Y. Liu, J. Tan, G. Owens and Z. Chen. 2018. Removal of Cr(VI) from aqueous solutions via reduction and absorption by green synthesized iron nanoparticles. *J. Clean. Prod*., 176: 929–936.

Katata-Seru, L., T. Moremedi, O.S. Aremu and I. Bahadur. 2018. Green synthesis of iron nanoparticles using Moringa oleifera extracts and their applications: Removal of nitrate from water and antibacterial activity against Escherichia coli. *J. Mol. Liq*., 256: 296–304.

Khan, S., M. Naushad, A. Al-Gheethi and J. Iqbal. 2021. Engineered nanoparticles for removal of pollutants from wastewater: Current status and future prospects of nanotechnology for remediation strategies. *J. Environ. Chem. Eng*., 9(5): 106160.

Khan, M.N. and L. Badshah. 2019. Floristic diversity and utility of flora of district Charsadda, Khyber Pakhtunkhwa. *Acta. Ecol. Sinica*, *39*(4): 306-320.

Lei, C., Y. Sun, D.C.W. Tsang and D. Lin. 2018. Environmental transformations and ecological effects of iron-based nanoparticles. *Environ. Pollut*., 232: 10-30.

LewisOscar, F., D. Mubarak Ali, C. Nithya, R. Priyanka, V. Gopinath, N.S. Alharbi and T. Thajuddin. 2015. One pot synthesis and anti-biofilm potential of copper nanoparticles (CuNPs) against clinical strains of *Pseudomonas aeruginosa*. *Biofouling*, 31(4): 379-391.

Lin, J., K. Nishino, M.C. Roberts, M. Tolmasky, R.I. Aminov and L. Zhang. 2015. Mechanisms of antibiotic resistance. *Front. Microbiol*., 6: 34.

Liu, X., L. Luo, Y. Ding and Y. Xu. 2011. Amperometric biosensors based on alumina nanoparticles-chitosan-horseradish peroxidase nanobiocomposites for the determination of phenolic compounds. *Analyst*, 136(4): 696-701.

Madivoli, E.S., P.G. Kareru, E.G. Maina, A.O. Nyabola, S.I. Wanakai and J.O. Nyang'au. 2019. Biosynthesis of iron nanoparticles using *Ageratum conyzoides* extracts, their antimicrobial and photocatalytic activity. *SN Appl. Sci*., 1(5): 500.

Makarov, V.V., S.S. Makarova, A.J. Love, O.V. Sinitsyna, A.O. Dudnik, I.V. Yaminsky, M.E. Taliansky and N.O. Kalinina. 2014. Biosynthesis of stable iron oxide nanoparticles in aqueous extracts of *Hordeum vulgare* and *Rumex acetosa plants*. *Langmuir*, 30(20): 5982-5988.

Manikandan, V., P. Jayanthi, A. Priyadharsan, E. Vijayaprathap, P.M. Anbarasan and P. Velmurugan. 2019. Green synthesis of pH-responsive Al2O3 nanoparticles: Application to rapid removal of nitrate ions with enhanced antibacterial activity. *J. Photochem. Photobiol. A: Chem*., 371: 205-215.

Manogar, P., J.E. Morvinyabesh, P. Ramesh, G.D. Jeyaleela, V. Amalan, J.S. Ajarem, A.A. Allam, J.S. Seong Khim and N. Vijayakumar. 2022. Biosynthesis and antimicrobial activity of aluminium oxide nanoparticles using *Lyngbya majuscula* extract. *Mater. Lett*., 311: 131569.

Manvitha, K. and B. Bidya. 2014. Review on pharmacological activity of *Cymbopogon citratus. Flora J*., 1(6): 5–7.

Mohamed, Y.M., A.M. Azzam, B.H. Amin and N.A. Safwat. 2015. Mycosynthesis of iron nanoparticles by *Alternaria alternata* and its antibacterial activity. *Afr. J. Biotechnol.*, 14(14): 1234-1241.

Monteiro-Riviere, N.A., S.J. Oldenburg and A.O. Inman. 2010. Interactions of aluminum nanoparticles with human epidermal keratinocytes. *J. Appl. Toxicol*., 30(3): 276-285.

Mukherjee, A., I.M. Sadiq, T. Prathna and N. Chandrasekaran. 2011. Antimicrobial activity of aluminium oxide nanoparticles for potential clinical applications. *Sci. Against Microbial Pathog*., 3(1): 212-215.

Muthukumar, H., S.N. Mohammed, N. Chandrasekaran, A.D. Sekar, A. Pugazhendhi and M. Matheswaran. 2019. Effect of iron doped Zinc oxide nanoparticles coating in the anode on current generation in microbial electrochemical cells. *Int. J. Hydrog. Energy*, 44(4): 2407-2416.

Muzammil, S., M. Khurshid, I. Nawaz, M.H. Siddique, M. Zubair, M.A. Nisar, M. Imran and S. Hayat. 2020. Aluminium oxide nanoparticles inhibit EPS production, adhesion and biofilm formation by multidrug-resistant *Acinetobacter baumannii*. *Biofouling*, 36(4): 492-504.

Nagarajan, P., V. Subramaniyan, V. Elavarasan, N. Mohandoss, P. Subramaniyan and S. Vijayakumar. 2023. Biofabricated aluminium oxide nanoparticles derived from *Citrus aurantium* L.: Antimicrobial, Anti-Proliferation, and Photocatalytic Efficiencies. *Sustainability*, 15(2): 1743.

Nagarajan, S. and K. Arumugam Kuppusamy. 2013. Extracellular synthesis of zinc oxide nanoparticles using seaweeds of Gulf of Mannar, India. *J. Nanobiotechnol*., 11(1): 39.

Olawade, D.B., O.Z. Wada, O. Fapohunda, B.I. Egbewole, O. Ajisafe and A.O. Ige. 2024. Nanoparticles for microbial control in water: Mechanisms, applications, and ecological implications. *Front. Nanotechnol*., 6: 1427843.

Parvekar, P., J. Palaskar, S. Metgud, R. Maria and S. Dutta. 2020. The minimum inhibitory concentration (MIC) and minimum bactericidal concentration (MBC) of silver nanoparticles against *Staphylococcus aureus*. *Biomater. Invest. Dent*., 7(1): 105-109.

Patiño-Ruiz, D., L. Sánchez-Botero, L. Tejeda-Benitez, J. Hinestroza and A. Herrera. 2020. Green synthesis of iron oxide nanoparticles using *Cymbopogon citratus* extract and sodium carbonate salt: Nanotoxicological considerations for potential environmental applications. *Environ. Nanotech. Monit. Manag*., 14: 100377.

Rossolini, G.M., F. Arena, P. Pecile and S. Pollini. 2014. Update on the antibiotic resistance crisis. *Curr. Opin. Pharmacol*., 18: 56-60.

Rufus, A., N. Sreeju, V. Vilas and D. Philip. 2017. Biosynthesis of hematite (α-Fe_2O_3) nanostructures: Size effects on applications in thermal conductivity, catalysis, and antibacterial activity. *J. Mol. Liq*., 242: 537-549.

Saeb, A.T.M., A.S. Alshammari, H. Al-Brahim and K.A. Al-Rubeaan. 2014. Production of silver nanoparticles with strong and stable antimicrobial activity against highly pathogenic and multidrug-resistant bacteria. *Sci. World J.*, 2014: 1-9.

Saleh, A.K., A.S. Shaban, M.A. Diab, D. Debarnot and A.S. Elzaref. 2023. Green synthesis and characterization of aluminum oxide nanoparticles using *Phoenix dactylifera* seed extract along with antimicrobial activity, phytotoxicity, and cytological effects on *Vicia faba* seeds. *Biomass Conv. Bioref*., 1-17.

Sarkar, B., A. Mahanty, S.K. Gupta, A.R. Choudhury, A. Daware and S. Bhattacharjee. 2022. Nanotechnology: A next-generation tool for sustainable aquaculture. *Aquaculture*, 546: 737330.

Sathiyavimal, S., S. Vasantharaj, D. Bharathi, M. Saravanan, E. Manikandan, S.S. Kumar and A. Pugazhendhi. 2018. Biogenesis of copper oxide nanoparticles (CuONPs) using *Sida acuta* and their incorporation over cotton fabrics to prevent the pathogenicity of Gram-negative and Gram-positive bacteria. *J. Photochem. Photobiol. B: Biol.*, 188: 126-134.

Sharma, P., J. Mack and A. Rojtman. 2013. Ten highly effective essential oils inhibit growth of methicillin-resistant *Staphylococcus aureus* (MRSA) and methicillin-sensitive *Staphylococcus aureus* (MSSA). *Int. J. Pharm. Pharmacol*., 5: 52-54.

Sumesh, K.R. and K. Kanthavel. 2019. Green synthesis of aluminium oxide nanoparticles and its applications in mechanical and thermal stability of hybrid natural composites. *J. Polym. Environ*., 27(10): 2189-2200.

Thahab, S.M., A.H. Abo Nasria and S. Hussain. 2020. Formation of Fe, Pt and (Pt/Fe) ultra-fine metal nanoparticles in different solution polarity prepared by Nd-YAG pulsed laser. *J. Phys. Conf. Ser*., 1535(1): 012040.

Ventola, C.L. 2015. The antibiotic resistance crisis: Part 1: Causes and threats. *Pharm. Ther.*, 40(4): 277.

Wahab, R. and M. Alam. 2022. Highly efficient and fast electrochemical sensor based on aluminium oxide (*Al2O3*) nanoparticle for the detection of organosulfur compounds. *Sens. Actuators A: Phys.*, 347: 113967.

Weinstein, M.P. and J.S. Lewis. 2020. The clinical and laboratory standards institute subcommittee on antimicrobial susceptibility testing: Background, organization, functions, and processes. *J. Clin. Microbiol.*, 58(3): e01864-19.

(Received for publication 11 July 2024)